



CrossMark
 click for updates

Cite this: *RSC Adv.*, 2015, 5, 32657

Thiazolo[5,4-*d*]thiazole-based organic sensitizers with strong visible light absorption for transparent, efficient and stable dye-sensitized solar cells†

Alessio Dessi,^{ab} Massimo Calamante,^{ab} Alessandro Mordini,^{ab} Maurizio Peruzzini,^a Adalgisa Sinicropi,^c Riccardo Basosi,^c Fabrizia Fabrizi de Biani,^c Maurizio Taddei,^c Daniele Colonna,^d Aldo di Carlo,^{de} Gianna Reginato^{*a} and Lorenzo Zani^{*a}

A small set of thiazolo[5,4-*d*]thiazole-based D- π -A organic dyes, endowed with *bis*-pentypropylenedioxythiophene (ProDOT) moieties in the π -spacer, was designed with the aid of computational analysis, synthesized and characterized. The presence of bulky and electronrich ProDOT groups beside the electron poor thiazolothiazole unit induced optimal physico-chemical properties, including broad and intense visible light absorption. As a consequence, the dyes were particularly suitable for application in thin layer dye-sensitized solar cells (TiO₂ thickness: 3.0–6.5 μ m). Small-scale (0.25 cm²) devices prepared using standard materials and fabrication techniques gave power conversion efficiencies up to 7.71%, surpassing those obtained with two different reference dyes. Transparent larger area cells (3.6 cm²) also showed good η values up to 6.35%, not requiring the use of a co-adsorbent, and retained their initial efficiency over a period of 1000 h storage at 85 °C. These results make this new family of organic sensitizers promising candidates for successful application in the production of efficient and stable transparent DSSCs for building-integrated photovoltaics.

Received 26th February 2015

Accepted 30th March 2015

DOI: 10.1039/c5ra03530a

www.rsc.org/advances

Introduction

Since their discovery in 1991,¹ dye-sensitized solar cells (DSSCs) have been widely regarded as a potential alternative to traditional silicon-based photovoltaic devices.^{2,3} In a DSSC, light harvesting takes place at the photoanode, constituted by a thin layer of a wide-band gap inorganic semiconductor (most often TiO₂) sensitized with a suitable dye: therefore, the choice of sensitizer plays a crucial role in determining the overall performances of the device.

Traditionally, DSSCs with high power conversion efficiencies (η) were first obtained with ruthenium metal-organic

sensitizers,⁴ whose performances were later surpassed by porphyrin dyes⁵ and, most recently, lead-containing perovskites.⁶ Fully organic sensitizers have also been employed, and efficiencies higher than 10%,^{7–9} sometimes even coupled with excellent stabilities,¹⁰ have been observed in such cases. The latter class of dyes presents some potential advantages compared to the other sensitizers, such as the possibility of not using precious or toxic metals, the ability to modify molecular properties by flexible synthetic procedures and the efficient harvesting of sunlight due to high molar absorptivities.¹¹

In particular, organic dyes with superior light absorption ability would be especially suitable for the sensitization of thin TiO₂ layers,¹² possibly useful for the development of solid-state DSSCs,¹³ but also for the construction of colored, transparent photovoltaic modules. The latter could find optimal application in the context of building-integrated photovoltaics (BIPV),¹⁴ currently considered one of the most appealing opportunities for DSSC commercialization.¹⁵

Another key point for a wide application of DSSCs has to deal with the simplification of fabrication techniques. It is well known that the application of surface treatments on both the conductive glass and the inorganic semiconductor, the consecutive deposition of multiple TiO₂ layers of different average particle size and shape,¹⁶ or the introduction of several additives and co-adsorbents both in the sensitizing baths and cell electrolytes¹⁰ are often required to obtain high efficiency. The discovery of new sensitizers able to give good performances

^aIstituto di Chimica dei Composti Organometallici (CNR-ICCOM), Via Madonna del Piano 10, 50019 Sesto Fiorentino (FI), Italy. E-mail: gianna.reginato@iccom.cnr.it; lorenzo.zani@iccom.cnr.it; Fax: +39 055 5225203; Tel: +39 055 5225245

^bDipartimento di Chimica "U. Schiff", Università degli Studi di Firenze, Via della Lastruccia 13, 50019 Sesto Fiorentino (FI), Italy

^cDipartimento di Biotecnologie, Università degli Studi di Siena, Chimica e Farmacia, Via A. Moro 2, 53100 Siena, Italy

^dDyepower Consortium, Viale Castro Pretorio 122, 00185 Rome, Italy

^eCenter for Hybrid and Organic Solar Energy (C.H.O.S.E.), Università degli Studi di Roma "Tor Vergata", Via del Politecnico 1, 00133 Rome, Italy

† Electronic supplementary information (ESI) available: Additional computational data, general synthetic remarks, synthesis and characterization of all new compounds, additional photoelectrochemical measurements, copies of the NMR spectra of compounds 7, 15, 19–20, 23, TTZ6 and 7. See DOI: 10.1039/c5ra03530a

under simplified conditions would allow to reduce the economic and environmental costs of DSSCs,¹⁷ thus helping to make this technology more sustainable.

In recent years, both we¹⁸ and others¹⁹ introduced new DSSC dyes featuring fused thiazole heterocycles as central electron withdrawing units. Among our compounds, sensitizer **TTZ1** (Fig. 1), having a thiazolo[5,4-*d*]thiazole (TzTz) core,²⁰ provided the best performances, with a maximum η of 3.53% obtained in the presence of chenodeoxycholic acid (CDCA) as a co-adsorbent.^{18a} We reasoned that the low efficiency observed for **TTZ1** could be attributed to a combination of factors, such as its limited light harvesting ability, its scarce solubility in most organic solvents and its tendency to form aggregates on TiO₂ surface, requiring the use of CDCA to improve photocurrents. Based on these considerations, we designed a new series of TzTz-containing sensitizers (see Fig. 1, **TTZ3–7**), with the precise aim to increase their visible light absorption and improve their solubility compared to **TTZ1**.

We supposed that replacement of the simple hexyl chains present in **TTZ1** with two alkoxy substituents could reduce the aromatic stabilization of the thiophene rings, thus slightly increasing the HOMO energies and decreasing the HOMO–LUMO gaps of the resulting molecules, ultimately leading to a red-shift of their absorption spectra. Moreover, a spectral red-shift and an improvement in light harvesting were expected by alternating the electronrich thiophene moieties with the electron withdrawing thiazolothiazole and cyanoacrylic units.²¹ Finally, placement of further alkyl chains on the sensitizers backbone was regarded as a way to improve their solubility,

which was considered beneficial both for their synthesis as well as their purification.

For these reasons, we replaced the 3-hexylthiophene units of **TTZ1** with bulkier and more electronrich *bis*-pentylpropylenedioxythiophene (ProDOT) moieties (**TTZ3**, Fig. 1).²² The design of such scaffold was supported by an accurate DFT computational analysis. We also modified the terminal triphenylamine group by introducing different substituents in *para*-position (**TTZ4–5**). The preparation and application of compounds **TTZ3–5** have been already reported by us in a recent preliminary communication.²³ To further modulate the electronic properties of the dyes and influence their photovoltaic performances, we decided to alter the conjugate portion of the compounds by inserting an electronrich ethylenedioxythiophene (EDOT) ring in place of the terminal thiophene present in **TTZ3–5** (**TTZ6**), and also to modify the terminal donor unit by replacing the triarylamine group with a phenothiazine moiety (**TTZ7**).

In addition to the previously reported data, herein we will disclose a full account describing the computational validation of compounds **TTZ3–7**, their detailed synthesis as well as their complete characterization. We will also report their use as sensitizers for thin-layer DSSCs under a variety of conditions (opaque/transparent semiconductor layers, presence/absence of additives, different layer thicknesses and surface areas, different electrolytes), and compare their performances with those of different reference sensitizers. Finally, the results of stability studies conducted under controlled conditions, as well as those of electrochemical impedance spectroscopy investigations, will be discussed.

Results and discussion

Computational analysis

Before starting our synthetic efforts, we analysed compounds **TTZ3–7** computationally. In the calculations, the alkyl chains present on the molecules were replaced by simple methyl groups to reduce the computational burden, without affecting the length and nature of the conjugate system.

Initially, structures were optimized *in vacuo* by means of DFT calculations at the B3LYP/6-31G* level;²⁴ the energy and shape of their frontier molecular orbitals (FMOs) were then compared with those previously found for dye **TTZ1**, which was used as a reference. Computed values of the HOMO–LUMO energy gaps for the **TTZ3–7** structures having both ProDOT rings in the most stable “chair” conformation are reported in Fig. 2, while the wave function plots of the FMOs are reported in Fig. S1 (ESI†).

Dye **TTZ3** showed a reduced HOMO–LUMO gap compared to **TTZ1** (2.11 eV vs. 2.17 eV), mostly due to HOMO destabilization. The HOMO energy increased even further and the frontier orbital gap decreased (1.95 eV) when the terminal triphenylamine unit was decorated with alkoxy substituents (**TTZ4**) to increase its electron donating character. In the case of dye **TTZ5**, alkylthio substituents were introduced on the donor moiety, since it was shown that their use could lead to DSSCs with improved V_{oc} and η compared to the oxygenated counterparts (for a discussion, *see below*).²⁵ The presence of such functional groups had a similar, but smaller effect on the HOMO energy,

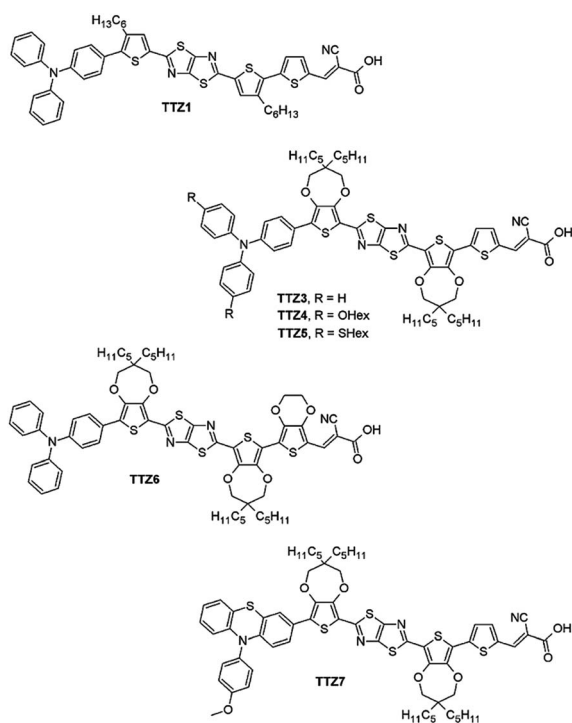


Fig. 1 Structure of previously described sensitizer **TTZ1** and of new dyes **TTZ3–7**.

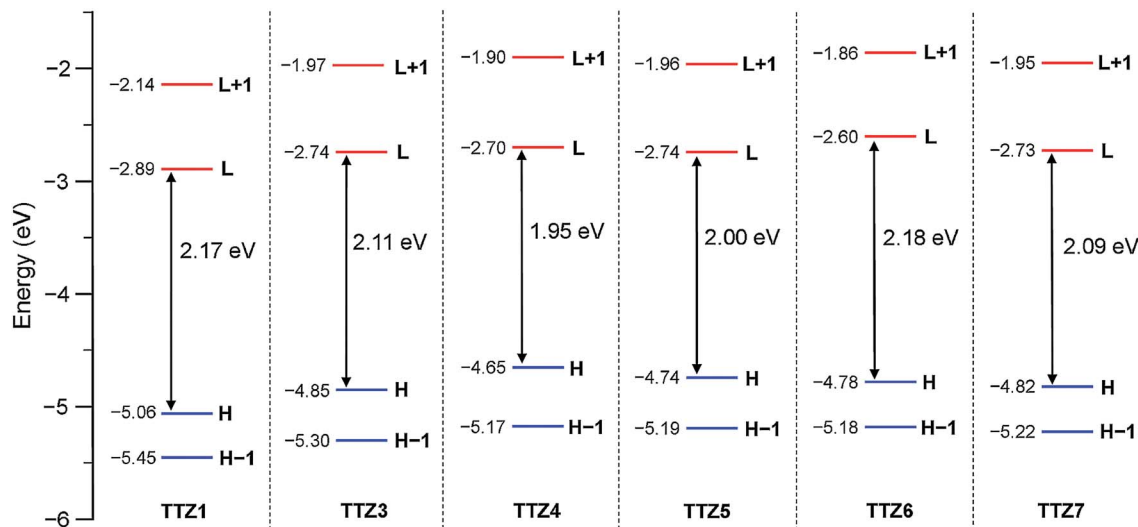


Fig. 2 Computed (B3LYP/6-31G*) HOMO–LUMO energy gaps of compounds TTZ1 and TTZ3–7.

resulting in a FMO gap of 2.00 eV. Compound **TTZ7**, bearing a phenothiazine donor moiety,²⁶ had a HOMO–LUMO gap comparable to that found for dye **TTZ3**, with a value of 2.09 eV. Finally, in the case of compound **TTZ6**, the presence of an EDOT group on the terminal portion made the molecule more electron-rich, in turn causing a significant LUMO destabilization without a big change of the HOMO energy. As a result, the FMO gap in this compound was larger than in dyes **TTZ3–5,7**, and closer to that found for **TTZ1** (2.17 vs. 2.18 eV). For all compounds, orbital shapes were similar, with the HOMO – 1 distributed along the entire conjugated system and the HOMO and LUMO mostly localized on the donor and acceptor moieties, respectively (Fig. S1†).

To learn more on the electronic transitions of the new organic sensitizers, the absorption maxima ($\lambda_{\text{max}}^{\text{a}}$), oscillator strengths (f) and vertical excitation energies (E_{exc}) in the most stable conformation were assessed by TD-DFT calculations in THF at the CAM-B3LYP/6-31G*²⁷ level (Table S1†). For all dyes the excitation process in the visible region results mostly from mixed HOMO → LUMO and HOMO – 1 → LUMO transitions. Interestingly, although **TTZ6** was the compound with the highest computed HOMO–LUMO gap, its excitation comprised a larger H → L fraction compared to the other dyes, resulting in a slightly red-shifted absorption maximum. In agreement with our expectations, computational results indicated that the new dyes should all have absorption maxima higher than 500 nm, red-shifted of approx. 20–30 nm relative to **TTZ1**; in addition, the higher oscillator strengths found for **TTZ3–7** suggested the possibility of more intense light absorption.

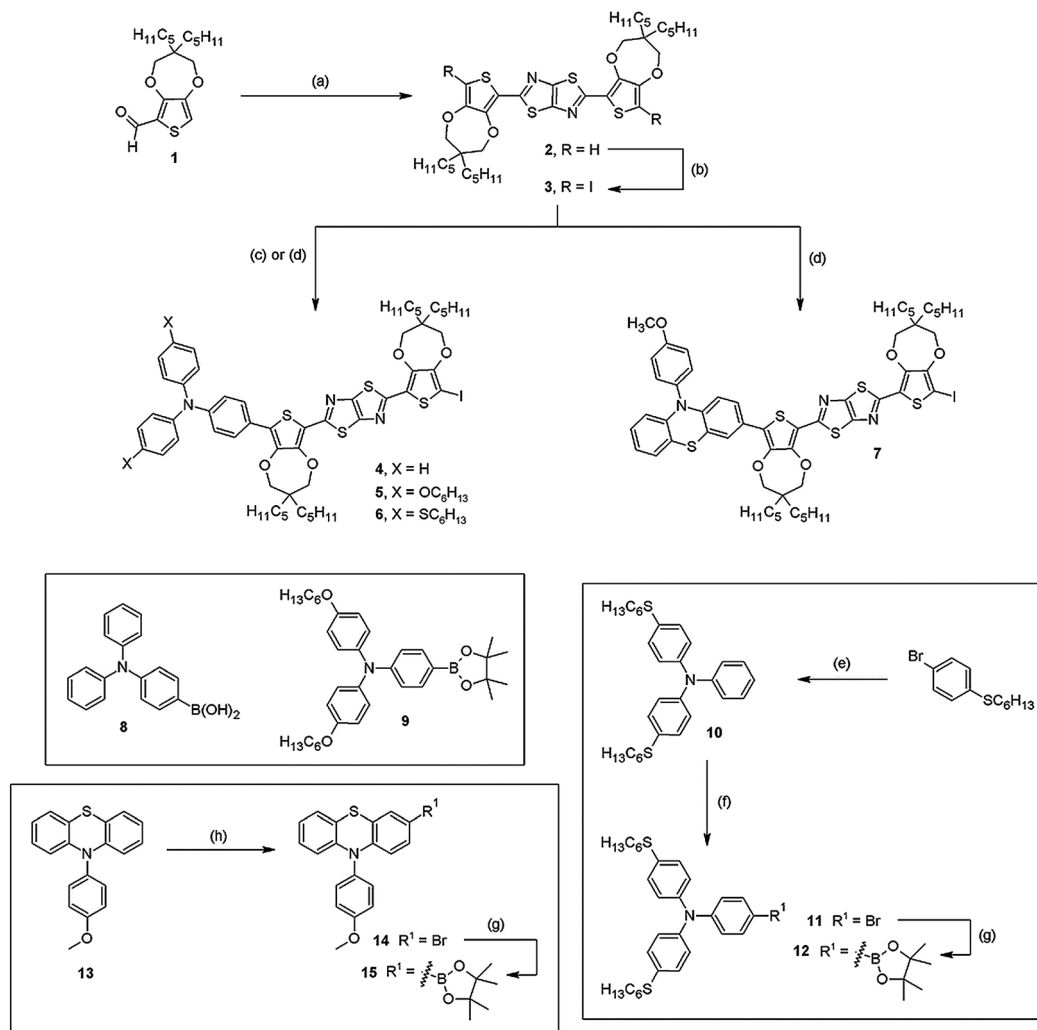
Synthesis of compounds TTZ3–7

The starting point of the synthesis of dyes **TTZ3–7** was constituted by aldehyde **1**, which was prepared in four steps following a reported procedure.²⁸ Compound **1** was converted to the corresponding thiazolo[5,4-*d*]thiazole (**2**) by reaction with

dithiooxamide under microwave activation (Scheme 1): initially, we carried out this transformation under the optimized conditions already established in our previously reported MW-assisted synthesis of thiazolothiazoles (nitrobenzene solution, 150 °C, 30 min).²⁹ However, we quickly realized that, due to the presence of the long alkyl chains on the ProDOT moieties, the product would not precipitate from the reaction mixture, thus complicating its separation from nitrobenzene. For this reason, we changed the solvent to *n*-BuOH³⁰ (facilitating chromatographic purification of **2**) and briefly optimized reaction temperature and time, ultimately obtaining the desired heterocyclic product in moderate yield.

After electrophilic halogenation with *N*-iodosuccinimide, the resulting *bis*-iodide **3** was subjected to Pd-catalyzed Suzuki cross-coupling with boronic acids/esters **8–9**, **12** and **15** to install the donor moieties. To minimize formation of the symmetrical double-coupling products, a stoichiometric amount of boronic reagent had to be employed, and the reaction had to be stopped before reaching full conversion, resulting in low yields of products **4–7**; despite that, a significant amount of unreacted diiodide **3** could usually be recovered after chromatographic purification for further reuse. Due to the lower reactivity of boronic esters **10** and **15**, an alternative protocol using [Pd(dppf)Cl₂] as the catalyst and KF as the base was employed instead of the classical procedure with Pd(PPh₃)₄.

Whereas boronic acid **8** is commercially available, and ester **9** was obtained *via* a reported procedure,³¹ compound **12** was prepared by the route shown in Scheme 1. First, Pd-catalyzed Buchwald–Hartwig reaction between 1-bromo-4-hexylthiobenzene^{32a} and aniline afforded triarylamine **10**, which was then brominated with *N*-bromosuccinimide (NBS) to yield compound **11**.^{32b} Finally, conversion of the latter to the corresponding boronic ester **12** was accomplished *via* Pd-catalyzed borylation, which proceeded with higher yield than the previously reported Li-mediated procedure.^{32b}



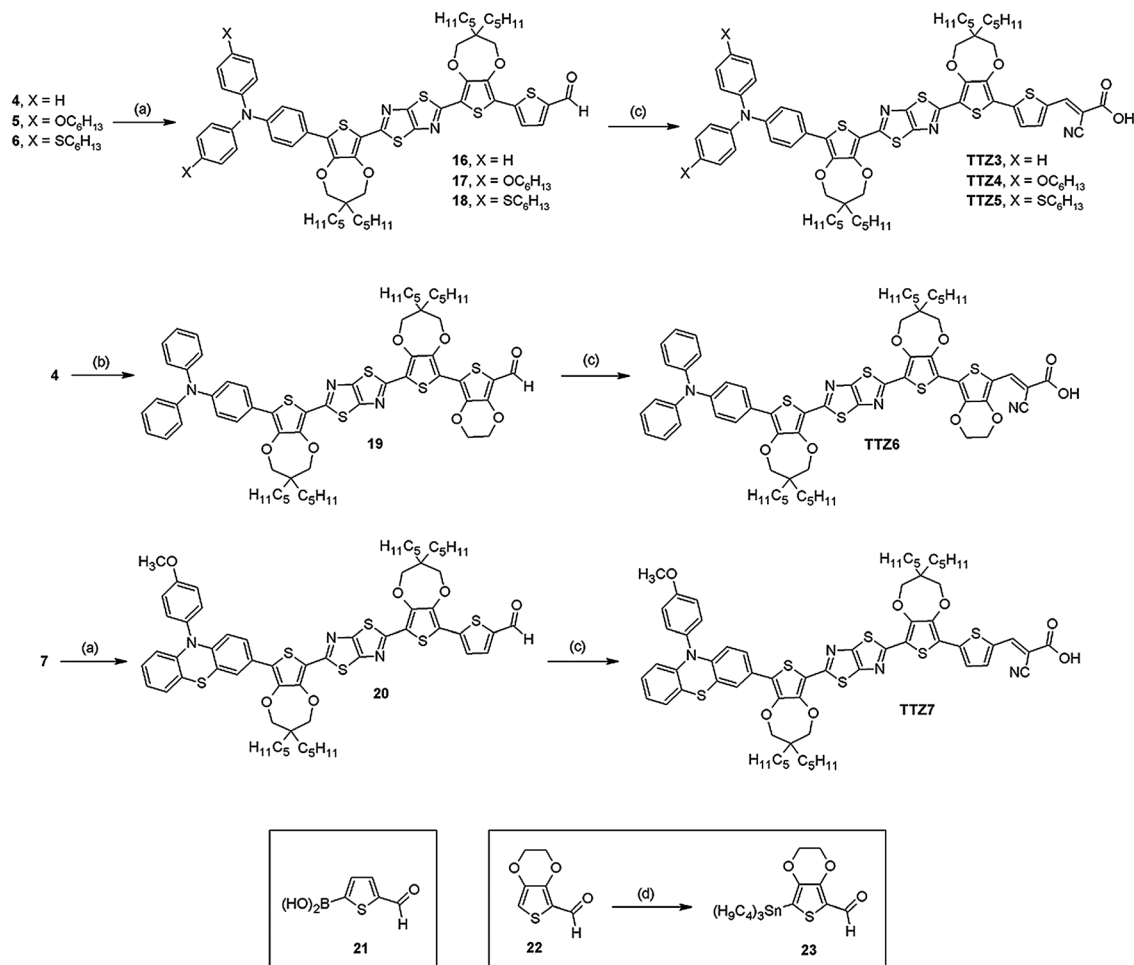
Scheme 1 Reagents and conditions: (a) dithioamide (0.5 eq.), *n*-BuOH, MW, 120 °C, 2.5 h then chloranil (0.25 eq.), THF, reflux, 10 min, 42%; (b) *N*-iodosuccinimide (2.5 eq.), $\text{CHCl}_3/\text{AcOH}$, rt, 16 h, 93%; (c) **8** or **9** (1.0 eq.), $\text{Pd}(\text{PPh}_3)_4$ (10 mol%), Na_2CO_3 (5.0 eq.), toluene, 100 °C, 16 h, 18–29%; (d) **12** or **15** (1.0 eq.), $[\text{Pd}(\text{dppf})\text{Cl}_2]$ (10 mol%), KF (5.0 eq.), toluene/EtOH, 78 °C, 5–16 h, 12–18%; (e) aniline (0.33 eq.), $\text{Pd}_2(\text{dba})_3 \cdot \text{CHCl}_3$ (5 mol%), dppf (10 mol%), *t*BuONa (1.33 eq.), toluene, reflux, 20 h, 80% (f) *N*-bromosuccinimide (1.0 eq.), CHCl_3 , rt, 4 h, 98% (g) $[\text{Pd}(\text{dppf})\text{Cl}_2]$ (10 mol%), *bis*-pinacolatodiboron (1.5 eq.), AcOK (3.0 eq.), *N,N*-DMF, 80 °C, 16 h, 60–83%; (h) PyHBr_3 (0.85 eq.), $\text{CH}_2\text{Cl}_2/\text{CH}_3\text{CN}$, rt, 30 min, 60%.

Reagent **15** was also prepared through a bromination/catalytic borylation sequence starting from known phenothiazine **13**.³³

However, initial electrophilic halogenation with typical reagents such as NBS and Br_2 under various conditions took place with limited success due to either lack of reactivity, or formation of *bis*-brominated derivatives. For this reason, we examined alternative reaction conditions, and ultimately employed a sub-stoichiometric amount of pyridinium bromide perbromide³⁴ to obtain a mixture of **13** and **14** in a 1 : 3 molar ratio, which could be used as such in the following step. Pd-catalyzed borylation of bromide **14** with *bis*(pinacolato)diboron then took place uneventfully, producing boronic ester **15** in good yield after chromatographic separation from unreacted **13**.

After preparation of intermediates **4–7**, the synthesis of dyes **TTZ3–7** was completed by introduction of the acceptor

moiety through a cross-coupling/Knoevenagel condensation sequence, with both processes proceeding in good to high yields (Scheme 2). In the case of compounds **TTZ3–5** and **TTZ7** the first reaction was a Suzuki coupling of iodides **4–7** with commercial boronic acid **21**: such transformation was activated by microwaves to shorten reaction times and limit the formation of by-products (for example deriving from protodehalogenation reactions). Stille cross-coupling of intermediate **4** with EDOT-containing stannane **23** was employed instead for dye **TTZ6**. Stannane **23** was prepared starting from known aldehyde **22** (ref. 35) by protection of the carbonyl group with trimethylorthoformate followed by lithiation of the resulting dimethylacetal and treatment with tributyltin chloride; at the end of the reaction, work-up with an aqueous solution of KHSO_4 led to deprotection of the formyl group, allowing isolation of compound **23**.



Scheme 2 Reagents and conditions: (a) **21** (1.5 eq.), [Pd(dppf)Cl₂] (5 mol%), KF (6.0 eq.), toluene/MeOH, MW, 70 °C, 30 min, 57–74%; (b) **23** (1.5 eq.), Pd(PPh₃)₄ (5 mol%), toluene, 110 °C, 24 h, 74%; (c) cyanoacetic acid (10.0 eq.), NH₄OAc (4.0 eq.), toluene/AcOH, 110 °C, 6 h, 84–97%; (d) CH(OMe)₃ (1.5 eq.), DDQ (5 mol%), CHCl₃/MeOH, 50 °C, 2 h then *n*-BuLi (1.5 eq.), Bu₃SnCl (2.0 eq.), THF, –78 °C to rt, 18 h, 67%.

Characterization of dyes TTZ3–7

In THF solution, all dyes showed broad and intense absorptions in the visible region (Fig. 3), with maxima in the 510–521 nm range, thus displaying a bathochromic shift of *ca.* 40–50 nm compared to **TTZ1**.^{18a} In agreement with the results of our computational analysis (*see above*), dyes **TTZ4** and **TTZ6** showed the most red-shifted absorption maxima; more generally, experimental excitation energies were quite close to the calculated values, with differences of at most 0.1 eV.

All dyes exhibited fluorescence in THF solution: therefore, optical band gaps (E_{0-0}) could be obtained from the intersection of the normalized absorption and emission spectra (Fig. S2†), and were comprised in the 2.14–2.25 eV range (Table 1), with **TTZ4** and **TTZ6** having the smallest E_{0-0} values. Such values were in good agreement with those derived from the corresponding Tauc plots,³⁶ which were found to be in the 2.12–2.16 eV range and in the same relative order (Fig. S3†).

When the dyes were attached to nanocrystalline TiO₂, they exhibited slightly broader and blue-shifted absorption spectra (21–27 nm), probably due to deprotonation of the carboxylic

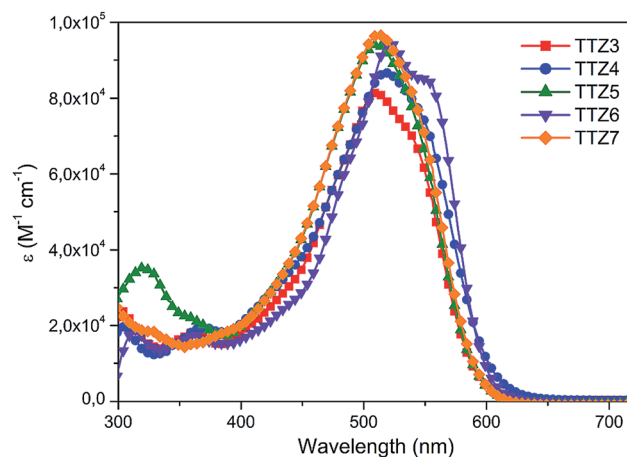


Fig. 3 UV-Vis spectra of dyes TTZ3–7 in THF solution. Concentrations: TTZ3, 8.47×10^{-6} M; TTZ4, 8.89×10^{-6} M; TTZ5, 8.96×10^{-6} M; TTZ6, 7.61×10^{-6} M; TTZ7, 9.57×10^{-6} M.

Table 1 Spectroscopic and electrochemical data for dyes TTZ3–5

Dye	$\lambda_{\max \text{ abs}}^a$ [nm] (ϵ [$\text{M}^{-1} \text{cm}^{-1}$])	$\lambda_{\max \text{ em}}^a$ [nm]	$\lambda_{\max \text{ abs. on TiO}_2}$ [nm]	E_{ox}^b [V]	$E_{\text{ox}}^*^c$ [V]	E_{0-0}^d [eV]	Γ [10^7 mol cm^{-2}]
TTZ3	510 (81 400)	587	484	1.02	-1.23	2.25	0.99
TTZ4	518 (86 600)	601	491	0.77	-1.42	2.19	1.08
TTZ5	510 (94 100)	573	487	0.91	-1.33	2.24	1.19
TTZ6	521 (94 500), 548 (85 100)	636	498	0.93	-1.21	2.14	1.25
TTZ7	513 (96 700)	596	492	0.85	-1.37	2.22	1.75

^a THF solution. ^b Potential vs. NHE. ^c Calculated from $E_{\text{ox}} - E_{0-0}$. ^d Estimated from the intersection of normalized absorption and emission spectra.

acid group on the semiconductor surface (Fig. 4).³⁷ The amount of dyes attached to TiO₂ was measured through the desorption method, by exposing electrodes sensitized with TTZ3–7 (similar to those later used for DSSC fabrication) to a 0.1 M KOH solution in THF/MeOH until complete discoloration, and measuring the absorbance of the resulting solution. The highest density was measured for TTZ7, but all dyes exhibited similar values in the $0.99\text{--}1.75 \times 10^{-7} \text{ mol cm}^{-2}$ range.

Ground-state oxidation potentials (E_{ox}) of all compounds were measured by means of cyclic voltammetry in CH₂Cl₂ solution (Fig. S4†). The strong electron-donating character resulting from introduction of the alkoxy groups on the triarylamine portion of TTZ4 was reflected by its relatively low E_{ox} value (0.77 eV vs. NHE); interestingly, also the presence of the terminal phenothiazine unit had a similar effect, with TTZ7 displaying a much lower oxidation potential compared to TTZ3. However, all the dyes had E_{ox} values positive enough to ensure regeneration by the iodide/triiodide redox shuttle.³⁸ Excited state oxidation potentials were obtained from the expression $E_{\text{ox}}^* = E_{\text{ox}} - E_{0-0}$, and were always found to be more negative than the conduction band edge of TiO₂ (approx. -0.5 V vs. NHE), confirming the possibility of smooth electron injection from the dye to the semiconductor during solar cell operation.

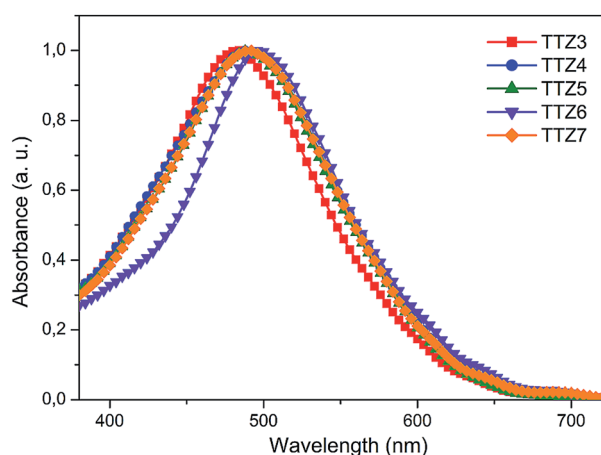


Fig. 4 Normalized UV-Vis spectra of dyes TTZ3–7 adsorbed on TiO₂.

Small-scale photovoltaic measurements

After characterization, compounds TTZ3–7 were employed as sensitizers in the construction of small-scale test DSSCs (0.25 cm² active surface, see Fig. 6a), aiming to evaluate their general level of performance and determine which one had the most promising photovoltaic properties.

In view of the very high molar extinction coefficients, suggesting the possibility of efficient light-harvesting, we reasoned that the new dyes could be conveniently used in DSSCs having a thinner TiO₂ layer compared to typical devices. For this reason, two series of cells were assembled: a first series with a transparent photoanode of 5.5 μm thickness (obtained with commercial Dyesol 18NR-T paste), and a second series with an opaque electrode of 6.5 μm thickness (Dyesol 18NR-AO).

We decided to keep device fabrication as simple as possible, as we reasoned that the efficiency data obtained under such simplified conditions could serve as a useful starting point to assess the potential of the new dyes in view of possible, more challenging, large-scale applications. In particular, no blocking layer of TiO₂ was deposited either on the conductive glass substrate or on the nanocrystalline semiconductor layer by treatment with aq. TiCl₄, and no light-scattering layer was employed in photoanode fabrication. Furthermore, differently from previous studies on thin-layer DSSCs,^{39,40} a commercial electrolyte solution based on the I⁻/I₃⁻ redox couple (Dyesol HPE) was used in the cells, since it usually gives optimal results with ruthenium sensitizers and is therefore still the most used for practical applications such as BIPV.

For both types of devices, performances obtained with the new sensitizers were compared with those of standard organic dye D5 (ref. 41 and 42) and Ru-based sensitizer Z907 (Fig. S5†).^{43,44} Typical J/V curves measured on the transparent solar cells are shown in Fig. 5a, while the corresponding IPCE spectra are displayed in Fig. 5b and the relevant photovoltaic parameters are reported in Table 2.

In the case of transparent cells, dyes TTZ3–7 gave efficiency values between 4.85 and 7.39%, with TTZ5 and TTZ7 being the best two sensitizers. Remarkably, all new thiazolo[5,4-*d*]thiazole dyes gave better efficiencies than standard organic dye D5, and the two most efficient compounds surpassed even the performance provided by ruthenium sensitizer Z907 (η 6.35–7.39% vs. 5.51%). This result was particularly significant, since Z907 is one of the sensitizers of choice for applications in BIPV.⁴⁵ All new compounds gave broad IPCE spectra with onsets around

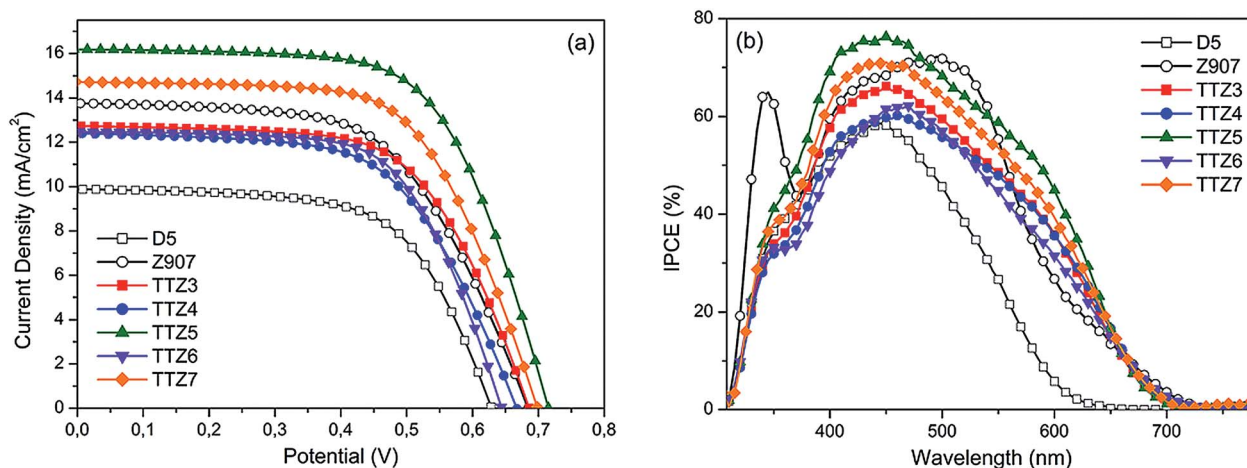


Fig. 5 Typical J/V curves (a) and IPCE spectra (b) for transparent cells built with dyes D5, Z907 and TTZ3–7.

Table 2 Photovoltaic parameters for DSSCs built with dyes D5, Z907 and TTZ3–7^a

Dye	Transparent DSSCs ^b					Opaque DSSCs ^c				
	CDCA ^d	J_{sc} [mA cm ⁻²]	V_{oc} [V]	FF [%]	η [%]	CDCA ^d	J_{sc} [mA cm ⁻²]	V_{oc} [V]	FF [%]	η [%]
D5	–	9.60	0.624	63	3.78	–	11.04	0.619	58	3.99
Z907	–	13.50	0.686	60	5.51	–	13.85	0.687	58	5.61
TTZ3	–	12.79	0.687	61	5.41	–	13.65	0.671	60	5.45
	+	15.62	0.697	60	6.55	+	16.52	0.683	58	6.54
TTZ4	–	12.18	0.669	60	4.85	–	12.99	0.665	57	4.93
	+	14.27	0.692	59	5.85	+	15.18	0.675	55	5.71
TTZ5	–	16.20	0.716	63	7.39	–	16.05	0.721	60	6.91
	+	16.59	0.717	59	7.08	+	18.33	0.709	59	7.71
TTZ6	–	12.29	0.646	63	5.01	–	13.00	0.644	56	4.70
	+	10.68	0.640	57	3.90	+	13.86	0.646	56	5.03
TTZ7	–	14.99	0.686	62	6.35	–	15.26	0.680	59	6.08
	+	15.97	0.694	60	6.61	+	17.22	0.689	58	6.94

^a Average values of three devices; active surface area 0.25 cm². ^b TiO₂ layer thickness 5.5 μm. ^c TiO₂ layer thickness 6.5 μm. ^d “–”: without CDCA; “+”: with 1 mM CDCA added in the sensitizing bath (0.1 mM dye in THF).

700 nm (Fig. 5b), in agreement with their UV-Vis spectra recorded on TiO₂; in particular, the IPCE of dye **TTZ5** was superior to **Z907** in the 370–480 and 550–660 nm regions, consistent with its higher photocurrent.

The improved performance of dye **TTZ5** compared to the other sensitizers could be attributed to the presence of an alkylthio-substituted triphenylamine moiety as the donor portion of the molecule. A conjugated dye bearing such donor group was investigated in detail by Berlinguette *et al.* and, as mentioned above, was found to induce superior photocurrent and photovoltage in DSSCs compared to its oxygenated analogue:²⁵ such effect was attributed to a 25-fold enhancement of the dye regeneration rate constant which, according to the authors, could either be due to formation of an adduct between iodide and the “soft” sulphur atoms, or simply result from the greater HOMO coefficients found on the S atoms compared to the O atoms. The latter observation is supported also by our

findings (compare the HOMO isodensity plots of **TTZ4** and **TTZ5** in Fig. S1,† and consider the higher J_{sc} and V_{oc} recorded for dye **TTZ5**).

The lower efficiencies recorded with the other dyes could be due to a combination of several factors, including lower light-harvesting efficiency (**TTZ3**, lowest molar absorptivity and dye density on TiO₂), insufficient dye regeneration (**TTZ4**, highest E_{ox} among all dyes) and increased recombination (**TTZ6**, larger HOMO coefficients on the terminal part of the molecule, see Fig. S1†).

Data obtained for opaque cells were generally consistent with those recorded for transparent devices (Table 2 and Fig. S6 and 7†), with **TTZ5,7** being once again the two best sensitizers, albeit with slightly reduced efficiency values (η 6.08–6.91%). Short-circuit current, open-circuit voltage and fill factor values were similar in the two classes of cells, reflecting the use of analogous fabrication conditions. The relatively low fill factors

observed for all cells (55–63%) were likely due to the small thickness of the TiO₂ layer employed, combined with the absence of a blocking layer, probably favouring electron recombination through direct contact between the conductive substrate and the electrolyte solution.

To verify if the tridimensional arrangement of alkyl chains on the ProDOT moieties²² was sufficient to suppress aggregation of the new dyes on TiO₂ surface, we also built two series of cells for which photoanode staining was carried out in the presence of 1 mM chenodeoxycholic acid (CDCA, Table 2 and Fig. S8 and 9†). In both device classes, an increase in J_{sc} was observed for all sensitizers, with the sole exception of **TTZ6**, perhaps due to the steric bulk of its terminal EDOT ring (minimizing aggregation even in the absence of CDCA), while the largest enhancement was displayed by dye **TTZ3** (+21–22%). This time, the best result was provided by **TTZ5**-containing opaque cells, which gave an average efficiency of 7.71% with a remarkable photocurrent of 18.33 mA cm⁻².

Fabrication and characterization of strip DSSCs

Following the promising results obtained with small-scale DSSCs (0.25 cm²), we decided to build larger area (3.6 cm²) strip cells (Fig. 6b), aiming to investigate how the increase in active surface could affect device efficiency and stability, in view of a possible scale-up of the system. Accordingly, we also introduced some changes in device fabrication. First, electrodes were prepared with two different thicknesses of transparent TiO₂, namely 3 and 5 μm, in order to minimize semiconductor employment and enhance transparency; secondly, a different commercial electrolytic solution (Dyesol HSE) was used, still based on the I⁻/I₃⁻ redox couple, which is designed to improve device stability at the cost of maximum performance. Finally, only dyes **TTZ3–5** were used in these experiments, due to their easier preparation procedure.

Again, for each electrode thickness, two series of cells were prepared, either by addition of CDCA in the sensitizing bath or not. The well-known organic dye **D35** (Fig. S5†) was selected as a reference,⁴⁶ since this compound has recently been established worldwide as a reference organic sensitizer for DSSCs, due to its good performances coupled with high transparency and excellent stability.⁴⁷ Typical J/V curves obtained for the CDCA-free and CDCA-containing strip cells are shown in Fig. 7a and b, respectively, while the relevant photovoltaic parameters are reported in Tables 3 and 4.

Although DSSCs with a thicker TiO₂ layer gave slightly improved performances compared to those with a thinner electrode, differences in efficiency were rather small. Predictably, thicker devices produced a higher photocurrent as a result of the larger amount of dye adsorbed on the anode, but at the same time their open-circuit voltages were smaller, probably due to higher electron recombination. Fill factors of these devices were generally lower than those of small-scale cells due to the higher series resistance usually observed for larger DSSCs.⁴⁸ However, it was really remarkable that all the three dyes **TTZ3–5** yielded more efficient devices than standard sensitizer **D35**, with the best result provided once again by **TTZ5** (6.35% average efficiency for the 5 μm device). The superior efficiencies were mostly due to the higher photocurrents of the thiazolo[5,4-*d*]thiazole-containing dyes compared to **D35**; such difference could be explained considering their wider (and in the case of **TTZ5** also higher) IPCE spectra, see Fig. S10–12.†

To our surprise, and in contrast to what was observed in the case of small-scale cells, the effect of CDCA on the performance of the larger-area devices (Table 4 and Fig. 7b) was that of giving lower efficiencies compared to the CDCA-free strip cells, with the sole exception of the 5 μm device built with dye **TTZ4**. In particular, no general improvement in photocurrent was observed in this second series of cells, highlighting a lower tendency of the dyes to aggregate under these conditions. Accordingly, we tentatively assume that when the standard 0.1 mM dye solution is used to sensitize the larger electrodes, a more homogeneous distribution of the sensitizer is achieved, minimizing stacking and other aggregation phenomena and thus eliminating the potential benefits brought by the co-adsorbent.

At this stage, the stability of the strip cells fabricated with dyes **TTZ3–5** (Fig. 8) was also tested. A new series of 3 μm-thick devices was built and their power conversion efficiencies measured under standard illumination over a period of approx. 1000 h, during which they were stored in the dark at 85 °C. All DSSCs showed excellent stability during this period of time, with final efficiencies comparable to the initial ones (for **TTZ4–5** a slight increase was even observed within the first 72 h). In particular for compound **TTZ5** the efficiency was steadily around 6% for the entire duration of the experiment, consistent with the results described above. Interestingly, while the short circuit current density had a small increase at the beginning of the experiment followed by a slow decrease, an opposite pattern was observed for the open circuit voltage, with an initial drop followed by a

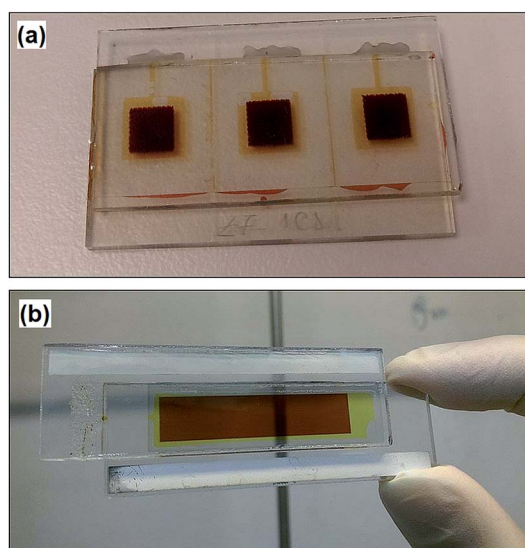


Fig. 6 (a) Small-scale dye-sensitized solar cells (active area 0.25 cm²) and (b) strip DSSCs (active area 3.6 cm²) used in this study.

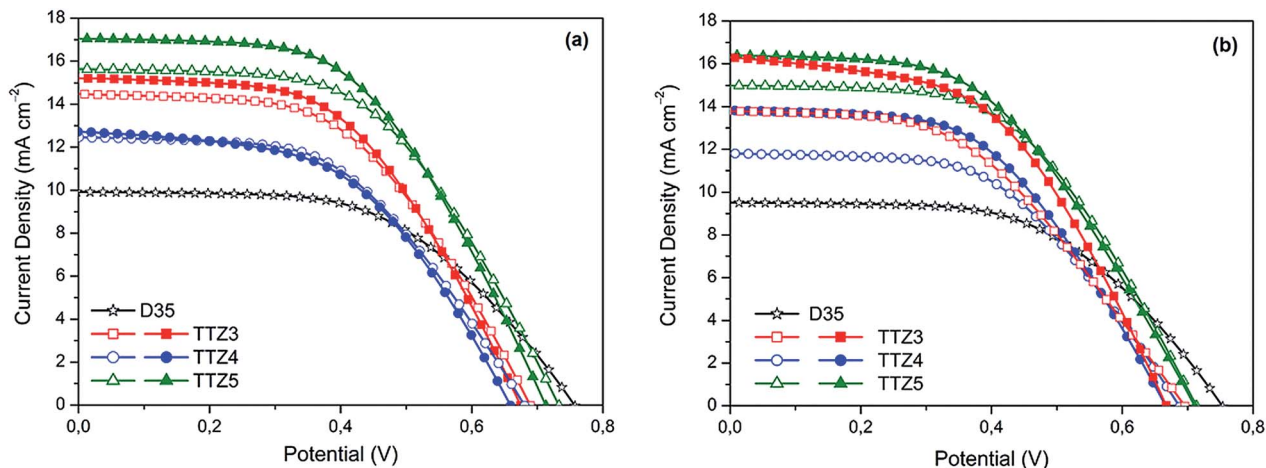


Fig. 7 Typical J/V curves for transparent strip cells built with dyes D35 and TTZ3–5 in the absence (a) and in the presence (b) of CDCA. Hollow symbols: 3 μm devices; full symbols: 5 μm devices.

Table 3 Photovoltaic parameters for strip DSSCs built with dyes D35 and TTZ3–5^a

Dye	Thickness [μm]	J_{sc} [mA cm^{-2}]	V_{oc} [V]	FF [%]	η [%]
D35	3	9.93	0.758	54	4.06
TTZ3	3	14.65	0.693	53	5.40
	5	15.70	0.678	52	5.58
TTZ4	3	13.14	0.682	52	4.70
	5	13.51	0.667	52	4.71
TTZ5	3	15.78	0.732	53	6.20
	5	17.00	0.705	53	6.35

^a Average values of two devices; active surface area 3.6 cm^2 .

Table 4 Photovoltaic parameters for strip DSSCs built with dyes D35 and TTZ3–5 with the addition of CDCA^a

Dye	Thickness [μm]	J_{sc} [mA cm^{-2}]	V_{oc} [V]	FF [%]	η [%]
D35	3	9.52	0.754	55	3.93
TTZ3	3	13.80	0.696	47	4.52
	5	16.31	0.667	50	5.48
TTZ4	3	12.62	0.690	52	4.55
	5	14.31	0.677	52	5.04
TTZ5	3	15.29	0.722	54	6.03
	5	16.38	0.711	50	5.88

^a Average values of two devices; active surface area 3.6 cm^2 ; 1.0 mM CDCA was added to the electrode sensitization bath.

subsequent recovery; similarly, fill factors increased slightly during the experiment. These results indicate that sensitizers of the thiazolothiazole series are promising candidates for the potential fabrication of large-scale thin-film DSSC modules due to their good performances coupled with high photochemical stability.

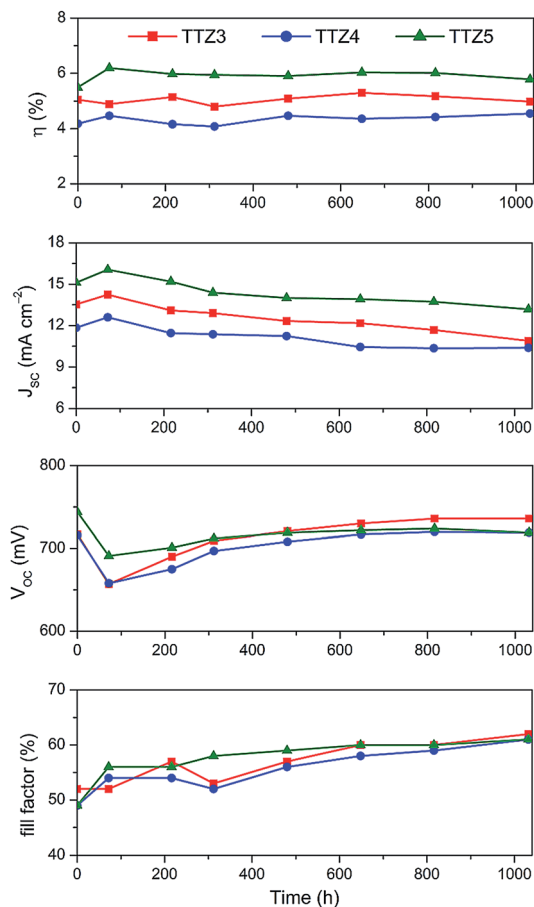


Fig. 8 Stability test conducted with 3 μm -thick DSSCs sensitized with dyes TTZ3–5 over the course of 1000 h. Ageing in the dark at 85 $^{\circ}\text{C}$.

Electrochemical impedance spectroscopy

In the final part of our studies, we analyzed more in detail the charge transfer processes taking place in the cells by means of electrochemical impedance spectroscopy (EIS).⁴⁹ Measurements

for **TTZ3**–5-containing strip cells (5 μm) were performed in the dark at -0.60 V forward bias over the 0.1 Hz–100 KHz frequency range: the corresponding Nyquist plots (*i.e.* the plots showing the minus imaginary part of the impedance $-Z''$ vs. the real part Z' when sweeping the frequency) are shown in Fig. 9a, while Bode phase plots (*i.e.* the plots showing the current/voltage phase shift vs. the frequency) are shown in Fig. 9b.

In the Nyquist plots, due to the use of a liquid electrolyte, two semicircles were observed: the small semicircle at higher frequencies corresponds to charge transfer processes at the Pt–electrolyte interface, while the larger semicircle at lower frequencies derives from the charge transfer processes at the TiO_2 –dye–electrolyte interface. Several parameters can be obtained by fitting the spectra with a known electrochemical model (see the equivalent circuit in Fig. 9c), namely the series

resistance of the cell (R_s), the charge transfer resistance at the TiO_2 –dye–electrolyte interface (R_{rec}) and the charge transfer resistance at the counter electrode (R_{CE}). Here, while R_s and R_{CE} were comparable for all dyes (reflecting the similar fabrication conditions and the same materials used in the counter electrode), R_{rec} values increased in the order **TTZ4** (22.0 Ω) < **TTZ3** (30.2 Ω) < **TTZ5** (37.2 Ω), suggesting that for the latter dye a slower charge recombination was taking place at the photoanode. Considering the Bode phase plots, the frequency of the peaks observed in the middle-frequency domain can be used to evaluate the electron lifetime within the semiconductor (τ_e),⁵⁰ providing another indication of the charge recombination rate. In agreement with the previous measurements, we found that electron lifetimes increased in the order **TTZ4** (15.1 ms) < **TTZ3** (17.5 ms) < **TTZ5** (23.2 ms), confirming that electron recombination was more efficiently prevented by the dye with the alkylthio-terminal chains. As recently pointed out in other studies,⁵¹ electron lifetime, influenced by factors such as molecular size and dye adsorption behaviour, exerts a strong influence on cell photovoltage. Indeed, also here, the trend in τ_e values was in good agreement with V_{oc} values measured for the cells and reported in Table 4.

Finally, we also measured EIS spectra at different potentials for all three dyes (see Fig. S13† for the corresponding Nyquist plots). As expected, with a decrease in the bias potential from -0.80 to -0.45 V the interfacial charge recombination process gave rise to a progressively larger semicircle in the mid-frequency region; at high potential, both interfacial charge transfer- and transport resistances within the TiO_2 became smaller due to the increased electron density, and a small feature at the lowest applied frequencies became visible as an effect of the diffusion of the I_3^- ions in the electrolyte.

Conclusions

In this work, five new thiazolo[5,4-*d*]thiazole-based organic dyes (**TTZ3**–7) were synthesized and characterized with the aim to use them as sensitizers in thin-layer DSSCs (TiO_2 thickness ≤ 6.5 μm). The new compounds displayed broad and intense absorption spectra in the visible region, with impressive molar absorptivities up to $9.67 \times 10^4 \text{ M}^{-1} \text{ cm}^{-1}$. Small-scale solar cells built with **TTZ3**–7, both transparent and opaque, gave good power conversion efficiencies (η up to 7.71%), which in the case of **TTZ5** and **TTZ7** were clearly superior to those obtained with standard Ru-dye **Z907**. Larger-scale strip cells (active area: 3.6 cm^2), featuring thin films of transparent TiO_2 (3–5 μm) and a high stability electrolyte, gave efficiencies in line with those obtained with the smaller devices, with **TTZ5** being once again the best sensitizer (η up to 6.35%). Remarkably, in this case employment of CDCA was not necessary, since addition of the co-adsorbent to the sensitizing bath did not lead to any improvement in cell efficiencies compared to the original devices. Even more importantly, all the dyes examined at this stage (**TTZ3**–5) led to solar cells with very high stability, as shown by a 1000 h storage test at 85 $^\circ\text{C}$, at the end of which efficiencies resulted practically unchanged compared to initial ones.

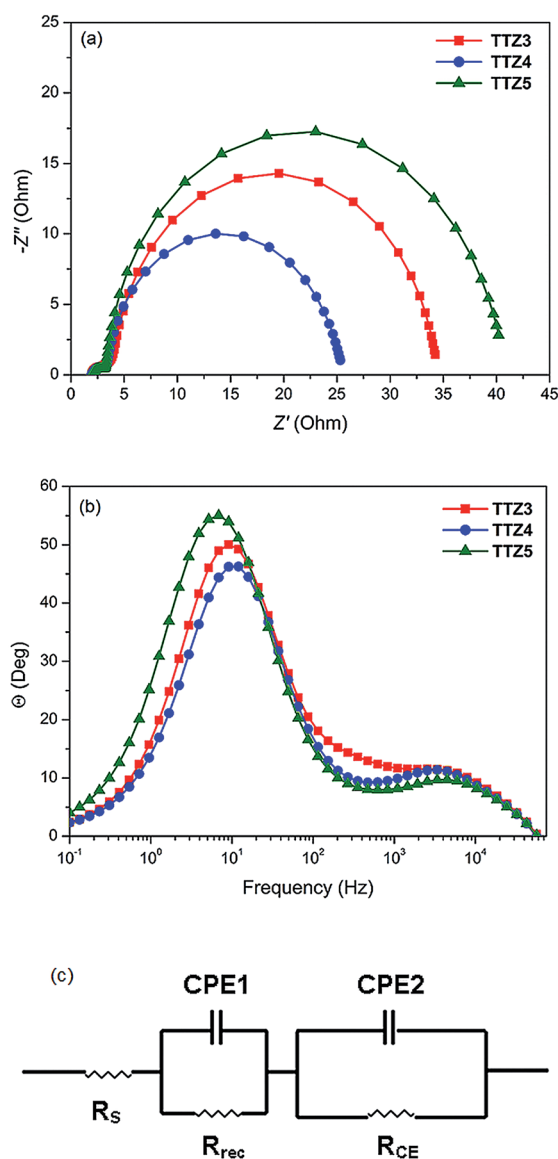


Fig. 9 Electrochemical impedance spectra for compounds **TTZ3**–5 measured in the dark at -0.60 V forward bias: (a) Nyquist plot; (b) Bode phase plot; (c) equivalent circuit.

Finally, the charge transfer processes within the cells were investigated by means of electrochemical impedance spectroscopy. These measurements indicated that dye **TTZ5** was able to minimize electron recombination from the semiconductor to the oxidized electrolyte more efficiently than the other sensitizers, resulting in a longer charge carrier lifetime and higher V_{oc} . Such data, coupled with the observation reported by Berlinguette *et al.* that dyes with alkylthio-substituted triphenylamine donor units are more efficiently regenerated compared to their oxygenated or unsubstituted analogs,²⁵ could contribute to explain the superior photovoltaic performances exhibited by dye **TTZ5** in comparison with the other sensitizers described in this study.

We are currently trying to expand our library of thiazolothiazole-based sensitizers and develop a synthetic procedure suitable for their large-scale preparation. The dyes will then be used in the fabrication of transparent, thin film DSSC modules to be subjected to even more demanding efficiency and stability measurements. The results of such investigations will be reported in due course.

Experimental

Transparent photoanodes for small-scale DSSCs were prepared by screen-printing a commercial TiO_2 paste (Dyesol 18NR-T) on a $8 \Omega \text{ sq}^{-1}$ conductive glass substrate (Pilkington), and by sintering the resulting electrodes at $520 \text{ }^\circ\text{C}$ for 30 minutes. After sintering, the thickness of the semiconductor layer was measured by means of a profiler (Dektak 150, Veeco) and determined to be $5.5 \mu\text{m}$. Opaque photoanodes were obtained following an analogous procedure, but using a different commercial titania paste (Dyesol 18NR-AO); their final thickness was $6.5 \mu\text{m}$. In both cases, the electrode active area was 0.25 cm^2 . Counter electrodes were obtained by screen printing a commercial platinum-containing paste (Chimet) on pre-drilled conductive glass plates and by heating at $420 \text{ }^\circ\text{C}$ for 15 minutes. TiO_2 photo-electrodes were sensitized by overnight immersion at rt into the appropriate dye solution (0.1 mM in THF for dyes **TTZ3–7**, 0.2 mM in EtOH for dye **D5**, 0.3 mM in EtOH for dye **Z907**), either in the absence or in the presence of 1 mM chenodeoxycholic acid (CDCA). After sensitization, the anodes were rinsed with EtOH and deionized water, and then dried. A TiO_2 -sensitized photoanode and a Pt counter electrode were assembled into a sealed sandwich-type cell using a $25 \mu\text{m}$ hot-melt Surlyn® gasket (Solaronix). A drop of the I^-/I_3^- containing commercial HPE electrolyte solution (Dyesol) was placed on the drilled hole on the back of the counter electrode and was driven into the cell by vacuum backfilling. The hole was finally sealed by using additional sealing film and a small glass cover. Fabrication of strip cells (3.6 cm^2 active area) was carried out following the same procedure, except that only transparent photoanodes were prepared, in a thickness of 3 and $5 \mu\text{m}$, and a different electrolyte (Dyesol HSE) was used to fill the cells. Sensitization of the photoanodes with standard sensitizer **D35** was performed using a 0.3 mM solution of the dye in 1-methoxy-2-propanol.

The devices underwent photovoltaic characterization by using a AM 1.5G solar simulator equipped with a Xenon lamp (KHS Solar Constant 1200). The measurements were performed with a power of incoming radiation of 100 mW cm^{-2} . J/V curves were obtained by applying an external bias to the cell and measuring the generated photocurrent with a Keithley model 2400 digital source-meter, under the control of dedicated LabTracer 2.0 software. A black shading mask was used to avoid overestimation of the measured parameters. IPCE spectra were measured with a dedicated apparatus built with the following components: Newport model 70612 Xenon lamp (150 W), Cornerstone 130 1/8 m monochromator and Keithley model 2400 digital source-meter.

Electrochemical impedance spectroscopy (EIS) measurements were performed in the dark using a AUTOLAB 302N potentiostat (Metrohm) equipped with a Nova electrochemical interface system, working at -0.80 V , -0.60 V and -0.45 V forward bias. The spectra were recorded over a frequency range of 10^{-1} Hz to 10^5 Hz with an amplitude of 10 mV. Data fitting was carried out using the EC-Lab software (V9.46).

Acknowledgements

The authors thank the “Ente Cassa di Risparmio di Firenze” foundation (“IRIS” project) and MIUR (“Progetto Premiale 2011: Produzione di Energia da Fonti Rinnovabili”) for financial support. A. S. and R. B. thank CINECA and CREA (Colle Val d’Elsa, Italy) for the availability of high performance computing resources and financial support. In addition, the authors wish to thank Dr Francesca De Rossi (C.H.O.S.E., Rome, Italy) for performing the EIS measurements.

Notes and references

- 1 B. O'Regan and M. Grätzel, *Nature*, 1991, **353**, 737–740.
- 2 *Dye-sensitized solar cells*, ed. K. Kalyanasundaram, EPFL Press, Lausanne, 2010.
- 3 A. Hagfeldt, G. Boschloo, L. Sun, L. Kloo and H. Pettersson, *Chem. Rev.*, 2010, **110**, 6595–6663.
- 4 Recent examples: (a) C. Y. Chen, M. Wang, J. Y. Li, N. Pootrakulchote, L. Alibabaei, C. H. Ngoc-le, J. D. Decoppet, J. H. Tsai, C. Grätzel, C. G. Wu, S. M. Zakeeruddin and M. Grätzel, *ACS Nano*, 2009, **3**, 3103–3109; (b) Y. Numata, S. P. Singh, A. Islam, M. Iwamura, A. Imai, K. Nozaki and L. Han, *Adv. Funct. Mater.*, 2013, **23**, 1817–1823.
- 5 L.-L. Li and E. W.-G. Diau, *Chem. Soc. Rev.*, 2013, **42**, 291–304.
- 6 (a) H. J. Snaith, *J. Phys. Chem. Lett.*, 2013, **4**, 3623–3630; (b) S. Kazim, M. K. Nazeeruddin, M. Grätzel and S. Ahmad, *Angew. Chem., Int. Ed.*, 2014, **53**, 2812–2825.
- 7 M. Zhang, Y. Wang, M. Xu, W. Ma, R. Li and P. Wang, *Energy Environ. Sci.*, 2013, **6**, 2944–2949.
- 8 J.-H. Yum, T. W. Holcombe, Y. Kim, K. Rakstys, T. Moehl, J. Teuscher, J. H. Delcamp, M. K. Nazeeruddin and M. Grätzel, *Sci. Rep.*, 2013, **3**, 2446.
- 9 J. Yang, P. Ganesan, J. Teuscher, T. Moehl, Y. J. Kim, C. Yi, P. Comte, K. Pei, T. H. Holcombe, M. K. Nazeeruddin, J. Hua, S. M. Zakeeruddin, H. Tian and M. Grätzel, *J. Am. Chem. Soc.*, 2014, **136**, 5722–5730.

- 10 K. Kakiage, Y. Aoyama, T. Yano, T. Otsuka, T. Kyomen, M. Unno and M. Hanaya, *Chem. Commun.*, 2014, **50**, 6379–6381.
- 11 Y. Ooyama and Y. Harima, *ChemPhysChem*, 2012, **13**, 4032–4080.
- 12 S. De Sousa, C. Olivier, L. Ducasse, G. Le Bourdon, L. Hirsch and T. Toupance, *ChemSusChem*, 2013, **6**, 993–996.
- 13 T. Miyasaka, *J. Phys. Chem. Lett.*, 2011, **2**, 262–269.
- 14 S. Yoon, S. Tak, J. Kim, Y. Jun, K. Kang and J. Park, *Build. Environ.*, 2011, **46**, 1899–1904.
- 15 H. Zervos, *Dye Sensitized Solar Cells (DSSC/DSC) 2013-2023: Technologies, Markets, Players*, IDTechEx Report, 2012, can be found at: <http://www.idtechex.com/research/reports/dye-sensitized-solar-cells-dssc-dsc-2013-2023-technologies-markets-players-000345.asp>.
- 16 S. Ito, T. N. Murakami, P. Comte, P. Liska, C. Grätzel, M. K. Nazeeruddin and M. Grätzel, *Thin Solid Films*, 2008, **516**, 4613–4619.
- 17 M. L. Parisi, S. Maranghi and R. Basosi, *Renewable Sustainable Energy Rev.*, 2014, **39**, 124–138.
- 18 (a) A. Dessì, G. Barozzino Consiglio, M. Calamante, G. Reginato, A. Mordini, M. Peruzzini, M. Taddei, A. Sinicropi, M. L. Parisi, F. Fabrizi de Biani, R. Basosi, R. Mori, M. Spatola, M. Bruzzi and L. Zani, *Eur. J. Org. Chem.*, 2013, 1916–1926; (b) L. Zani, G. Reginato, A. Mordini, M. Calamante, M. Peruzzini, M. Taddei, A. Sinicropi, M. L. Parisi, F. Fabrizi de Biani, R. Basosi, A. Cavallaro and M. Bruzzi, *Tetrahedron Lett.*, 2013, **54**, 3944–3948.
- 19 W. Zhang, Q. Feng, Z.-S. Wang and G. Zhou, *Chem.-Asian J.*, 2013, **8**, 939–946.
- 20 (a) D. Bevk, L. Marin, L. Lutsen, D. Vanderzande and W. Maes, *RSC Adv.*, 2013, **3**, 11418–11431; (b) L. Zani, M. Calamante, A. Mordini and G. Reginato, in *Targets in Heterocyclic Systems*, ed. O. A. Attanasi and D. Spinelli, Società Chimica Italiana, Rome, 2014, vol. 17, pp. 87–124.
- 21 B. G. Kim, K. Chung and J. Kim, *Chem.-Eur. J.*, 2013, **19**, 5220–5230.
- 22 Y. Liang, B. Peng, J. Liang, Z. Tao and J. Chen, *Org. Lett.*, 2010, **12**, 1204–1207.
- 23 A. Dessì, M. Calamante, A. Mordini, M. Peruzzini, A. Sinicropi, R. Basosi, F. Fabrizi de Biani, M. Taddei, D. Colonna, A. Di Carlo, G. Reginato and L. Zani, *Chem. Commun.*, 2014, **50**, 13952–13955.
- 24 (a) A. D. J. Becke, *J. Chem. Phys.*, 1993, **98**, 5648–5652; (b) C. Lee, W. Yang and R. G. Parr, *Phys. Rev. B: Condens. Matter Mater. Phys.*, 1988, **37**, 785–789; (c) P. J. Stephens, F. J. Devlin, C. F. Chabalowski and M. J. Frisch, *J. Phys. Chem.*, 1994, **98**, 11623–11627.
- 25 K. C. D. Robson, K. Hu, G. J. Meyer and C. P. Berlinguette, *J. Am. Chem. Soc.*, 2013, **135**, 1961–1971.
- 26 H. Tian, X. Yang, R. Chen, Y. Pan, L. Li, A. Hagfeldt and L. Sun, *Chem. Commun.*, 2007, 3741–3743.
- 27 T. Yanai, D. Tew and N. Handy, *Chem. Phys. Lett.*, 2004, **393**, 51–57.
- 28 B. C. Thompson, Y.-G. Kim, T. D. McCarley and J. R. Reynolds, *J. Am. Chem. Soc.*, 2006, **128**, 12714–12725.
- 29 A. Dessì, M. Calamante, A. Mordini, L. Zani, M. Taddei and G. Reginato, *RSC Adv.*, 2014, **3**, 1322–1328.
- 30 R. Ziessel, A. Nano, E. Heyer, T. Bura and P. Retailleau, *Chem.-Eur. J.*, 2013, **19**, 2582–2588.
- 31 L. Chen, B. Zhang, Y. Cheng, Z. Xie, L. Wang, X. Jing and F. Wang, *Adv. Funct. Mater.*, 2010, **20**, 3143–3153.
- 32 (a) C. G. Bates, R. K. Gujadhur and D. Venkataraman, *Org. Lett.*, 2002, **4**, 2803–2806; (b) K. C. D. Robson, B. D. Koivisto and C. P. Berlinguette, *Inorg. Chem.*, 2012, **51**, 1501–1507.
- 33 Y.-H. Seo, W.-H. Lee, J.-H. Park, C. Bae, Y. Hong, J.-W. Park and I.-N. Kang, *J. Polym. Sci., Part A: Polym. Chem.*, 2012, **50**, 649–658.
- 34 C. Djerassi and C. R. Scholz, *J. Am. Chem. Soc.*, 1948, **70**, 417–418.
- 35 A. K. Mohanakrishnan, A. Hucke, M. A. Lyon, M. V. Lakshmikantham and M. P. Cava, *Tetrahedron*, 1999, **55**, 11745–11754.
- 36 (a) J. Tauc, *Mater. Res. Bull.*, 1968, **3**, 37–46, application on molecular dyes; (b) C. Coluccini, N. Manfredi, M. M. Salamone, R. Ruffo, M. G. Lobello, F. De Angelis and A. Abboto, *J. Org. Chem.*, 2012, **77**, 7945–7956.
- 37 Y. J. Chang and T. J. Chow, *J. Mater. Chem.*, 2011, **21**, 9523–9531.
- 38 G. Boschloo and A. Hagfeldt, *Acc. Chem. Res.*, 2009, **42**, 1819–1826.
- 39 Z. Wang, M. Liang, L. Wang, Y. Hao, C. Wang, Z. Sun and S. Xue, *Chem. Commun.*, 2013, **49**, 5748–5750.
- 40 X. Wang, J. Yang, H. Yu, F. Li, L. Fan, W. Sun, Y. Liu, Z. Y. Koh, J. Pan, W.-L. Yim, L. Yan and Q. Wang, *Chem. Commun.*, 2014, **50**, 3965–3968.
- 41 D. P. Hagberg, T. Edvinsson, T. Marinado, G. Boschloo, A. Hagfeldt and L. Sun, *Chem. Commun.*, 2006, 2245–2247.
- 42 D. P. Hagberg, T. Marinado, K. M. Karlsson, K. Nonomura, P. Qin, G. Boschloo, T. Brinck, A. Hagfeldt and L. Sun, *J. Org. Chem.*, 2007, **72**, 9550–9556.
- 43 L.-P. Heiniger, P. G. O'Brien, N. Soheilnia, Y. Yang, N. P. Kherani, M. Grätzel, G. A. Ozin and N. Tétrault, *Adv. Mater.*, 2013, **25**, 5734–5741.
- 44 P. Wang, S. M. Zakeeruddin, J. E. Moser, M. K. Nazeeruddin, T. Sekiguchi and M. Grätzel, *Nat. Mater.*, 2003, **2**, 402–407.
- 45 L. Schmidt-Mende, J. E. Kroeze, J. R. Durrant, M. K. Nazeeruddin and M. Grätzel, *Nano Lett.*, 2005, **5**, 1315–1320.
- 46 D. P. Hagberg, X. Jiang, E. Gabrielsson, M. Linder, T. Marinado, T. Brinck, A. Hagfeldt and L. Sun, *J. Mater. Chem.*, 2009, **19**, 7232–7238.
- 47 Dye D35 is commercially available from Dyenamo AB (Sweden). For a list of references regarding applications of such dye, see: http://www.dyenamo.se/dyenamo_dyes.php.
- 48 Y. Huang, S. Dai, S. Chen, C. Zhang, Y. Sui, S. Xiao and L. Hu, *Appl. Phys. Lett.*, 2009, **95**, 243503.
- 49 F. Fabregat-Santiago, G. Garcia-Belmonte, I. Mora-Seró and J. Bisquert, *Phys. Chem. Chem. Phys.*, 2011, **13**, 9083–9118.
- 50 Q. Li, L. Lu, C. Zhong, J. Huang, Q. Huang, J. Shi, X. Jin, T. Peng, J. Qin and Z. Li, *Chem.-Eur. J.*, 2009, **15**, 9664–9668.
- 51 L. Yang, Z. Zheng, Y. Li, W. Wu, H. Tian and Z. Wang, *Chem. Commun.*, 2015, **51**, 4842–4845.